Egyptian Journal of Chemistry

http://ejchem.journals.ekb.eg/

Fabrication And Characterization Of Amorphous Si/Al/Ag Multilayers For Optoelectronic Devices

H. El-Desouky,[a] S. Hassan,[a] A. El -Shaer,[b] M. S. Abo Ghazala,[a] T.Y. Elrasasi*[c]

[a]*Faculty of Science, Menoufia University, Shebin El-Koom, Menoufia, 32511, Egypt*
[b]*Faculty of Science, Kafrelshiekh University, Kafr Elshaikh, Egypt.*
[c]*Physics department, Faculty of Science. Benha Univesity, Benha, Egypt.*

Abstract

Multilayer thin films of a-Si/Si, a-Si/Ag, and a-Si/Al/Ag were prepared on quartz substrates via thermal evaporation techniques followed by annealing at 500°C for one hour at low vacuum. The thermal, optical, and electrical measurements were investigated using TGA, U-V spectrophotometer, and RLC circuit. The results showed an oxidation occurrence during annealing for all samples. The results of the optical properties, such as the extinction coefficient and refractive index, revealed enhancements attributable to oxidation and the transition is direct to the band gap around 1.5 eV. The electrical properties were assessed by analyzing AC conductivity within the frequency range of 100 Hz to 500 kHz across different temperatures (300 to 370 K)., The results of AC indicate the presence of two conduction mechanisms -hopping and tunneling- dependent on frequency, temperature, and oxidation. Additionally, the I-V characteristic curves of the samples exhibited ohmic behavior, with resistance decreasing under light illumination suggesting potential applications in optoelectronic devices.

Keywords: Optoelectronics; amorphous silicon-metal multilayers; surface Plasmon's; hopping and tunneling conduction

1. Introduction

Optoelectronics is a rapidly advancing field, pivotal in the development of cutting-edge technologies such as telecommunications and solar energy harvesting. The pursuit of advanced materials for optoelectronic applications has gained considerable attention in recent years, driven by the need for improved performance and new functionalities [1,2]. This field enables the creation of high-speed, high-performance devices including lasers, radiation detectors, optical modulators, and displays [3].

A particularly promising area of research involves amorphous silicon-metal multilayers, which exhibit exceptional optoelectronic properties. These multilayer structures are valued for their ability to control light-matter interactions and their tunable optical and electrical properties, making them ideal for applications in photonics, sensing, and energy conversion. However, the performance and stability of these multilayers are highly dependent on their fabrication methods and external factors such as oxidation. Exposure to oxygen-rich environments can alter the optical and electrical properties of the materials, impacting device performance. Therefore, understanding the oxidation mechanisms and their effects on amorphous silicon-metal multilayers is crucial for optimizing performance and ensuring long-term reliability [4,5].

Optoelectronic devices made from amorphous silicon-metal multilayers can be fabricated using various methods, including chemical vapor deposition (CVD) and physical vapor deposition (PVD). The PVD technique, in particular, allows for precise control over the thickness and composition of each layer within the multilayer stack [6], which is essential for achieving the desired optical response. The combination of amorphous silicon with metals like aluminum (Al) and Tin (Sn) was deposited on quartz substrate by thermal evaporation deposition [7-9]. Silicon serves as a spacer layer, influencing the propagation length and confinement of surface plasmons on metal surfaces [10]. Metals like Al and Ag exhibit strong plasmonic resonances in specific wavelength ranges, and incorporating them into the multilayer can tailor the overall plasmonic response of the device [11,12].

Hopping and tunneling mechanisms are critical for understanding charge transport in these structures. Hopping refers to the movement of charge carriers (electrons or holes) in disordered systems by jumping between

localized states, which is essential in amorphous materials and disordered semiconductors [13,14]. Tunneling, a quantum mechanical phenomenon, involves particles passing through a potential barrier they classically could not overcome and is vital in many nanoscale electronic devices [15].

In this paper, the optoelectronic properties of silicon-aluminum-silver multilayers prepared by the thermal evaporation technique at the high vacuum are investigated.

2. Experimental
2.1. Materials and preparation methods

High-purity pellets of Si, Ag, and Al (99.99% purity) were obtained from Sigma-Aldrich. These metal layers were deposited onto a silicon substrate using the thermal evaporation technique. The deposition was carried out at a high vacuum maintained at 2×10^{-5} mbar. This procedure produced multilayers of varying thicknesses of 108 nm. The thickness of each layer was measured using a quartz crystal monitor (MAXTEK INC TM-100), which recorded thicknesses for Si/Si (40nm), Si/Ag (75nm), and Si/Al/Ag (108.5nm). Following the deposition process, all multilayers were annealed in a vacuum of 2×10^{-3} mbar at 500 °C for one hour, see Fig. (1).

2.2. Measurements

The prepared samples were rigorously examined using several techniques. (EDX), QUANTA FEG 250 instrument, energy dispersive x-ray spectroscopy have been used to identify the elements present in samples. The TGA of the mass spectrometer measures mass changes, the samples have been tested thermally from 40 °C up to 1000 °C with a heating rate of 10 °C/min for multilayers, TGA experiments were carried out by Netzsch (STA 449C and QMS 403C).
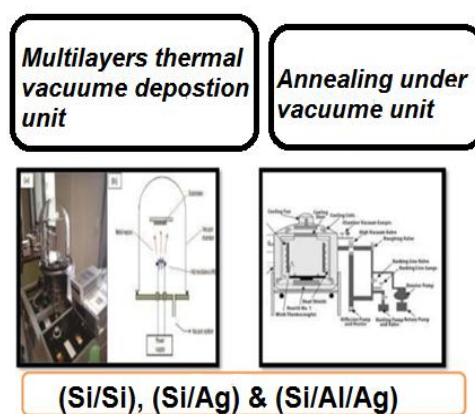

Fig. 1 Process and underlying mechanism for the creation of polycrystalline silicon thin films, utilizing a triple wire boat within a thermal vacuum evaporation system, annealing unit, and surface plasmons.

UV-VIS spectrophotometer (JASCO V-570) was utilized, covering a spectral range from 200 to 1100 nm to understand the optical characteristics of the films. AC conductivity measurements were performed PM6304 programmable automatic RCL (Philips) meter is used to determine dielectric and electrical measurements. It involved a cell comprising two probe electrodes and a nickel-chrome resistance heater within a range of 300 - 373 K, with frequency ranges between 100 HZ and 500 kHz. Current-voltage characteristics of the devices were measured using a two-electrode method with a Keithley Source Meter (type 2420), the samples were sandwiched between two brass electrodes.

3. Results and Discussion

Fig. (2) shows the EDX pattern displays Si/Si, Si/Ag, and Si/Al/Ag films, deposited on the quartz substrates and annealed at 500°C for one hour. The information obtained from the EDX analysis is presented in Table 1. It is seen that the appearance of oxygen content is due to oxidation of the samples during annealing suggesting that partial vacation which allows oxygen to penetrate samples causes an eutectic phase transition of various SiO_2 phases as the following reaction Eq. (1)

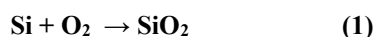$$Si + O_2 \rightarrow SiO_2 \qquad (1)$$

_____

Table (1): elements percentages of Si/Si, Si/Ag, and Si/Al/Ag multilayers.

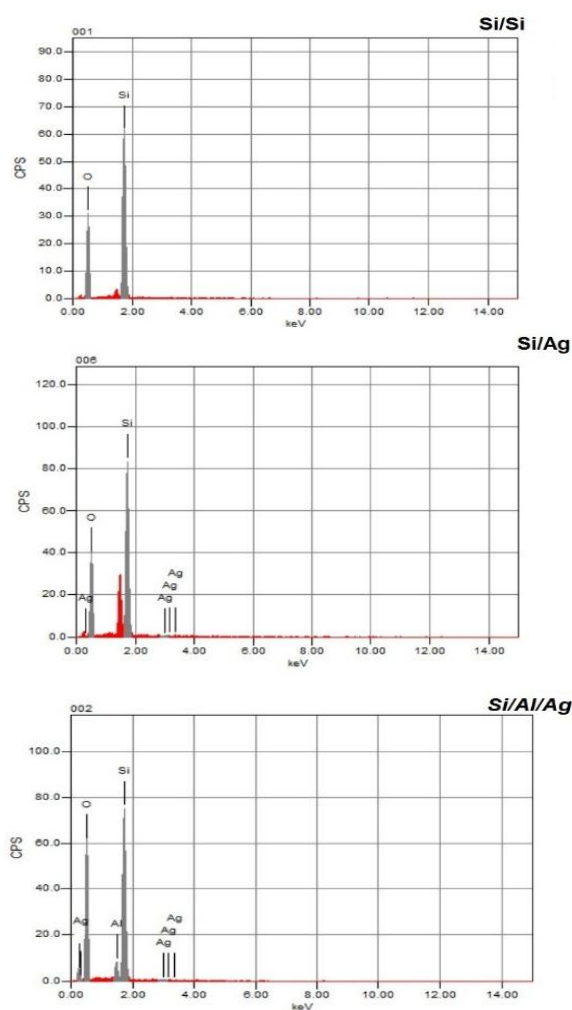|	Element	Si/Si	Si/Ag	Si/Al/Ag
	Si	41.85	39.84	32.92
Weight %	Al	-	-	4.13
	Ag	-	1.23	3.35
	O	58.15	58.93	59.6

Fig. 2 EDX pattern for Si/Si, Si/Ag, and Si/Al/ Ag multilayers annealed at 500 °C.

The TGA curves of Si/Si, Si/Ag, and Si/Al/ Ag multilayers are shown in Fig (3) which exhibit characteristic steps corresponding to the oxidation. The TGA analysis was used to study the thermal stability of our samples and determine the change in mass of the Si/Al/Ag multilayer as a function of temperature. To elucidate the kinetics of oxygen absorption in free-standing Si/Si, Si/Ag, and Si/Al/Ag layers, the mass increase was observed over   380 °C and 513 °C for all samples. For Si/Al/Ag multilayers, the TGA curve would typically show weight gain due to more oxidation, especially of the aluminum layer, as it forms aluminum oxide (Al_2O_2) when exposed to oxygen at elevated temperatures. This oxidation process often occurs in multiple stages, starting with the surface oxidation and potentially progressing to deeper layers if the temperature is sufficiently high. The effects of oxidation have been confirmed by EDX and FT-IR as shown in data of EDX, revealing the formation of different SiO_2 phases (see Eq.1) and O-H group in FTIR analysis, see our previous work [16,17].
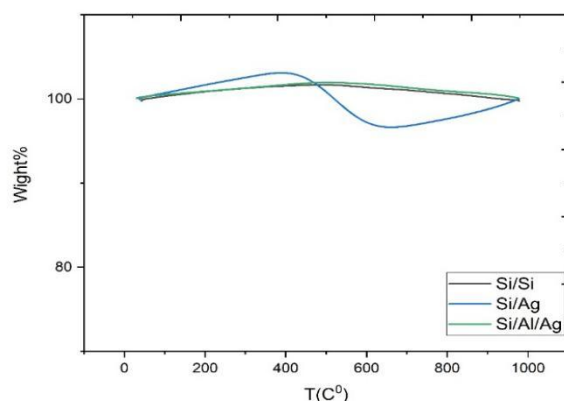
_____

Fig. 3 Thermo gravimetric analysis (TGA) isotherms of oxygen absorption at different temperatures for Si/Si, Si/Ag, and Si/Al/Ag.

The transmittance spectra of the multilayers annealed at 500 °C for one hour, in the wavelength range of 200–1100 nm are shown in Fig. (4). The values of transmittance for Si/Si samples increase by incorporation of Ag and Al metals due to the oxidation of Ag and Al in addition to Si as a result of the appearance of localized surface Plasmons [18] Surface plasmon resonance (SPR) is a phenomenon that occurs where electrons in a thin metal sheet become excited by light. Therefore, the maximum transmittance spectra for such multilayers are conditioned by the existence of bulk absorption modes according to their dispersion equation.

The absorption spectrum of multilayers is shown in Fig. (5). The absorbance positions appeared for Si/Si, Si/Ag, and Si/Al/Ag multilayers The values of transmittance for Si/Si samples decrease by incorporation of Ag and Al metals due to the oxidation of Ag and Al in addition to Si as a result of the appearance of localized surface Plasmons [19]. Therefore, the maximum transmittance spectra for such multilayers are conditioned by the existence of bulk absorption modes.
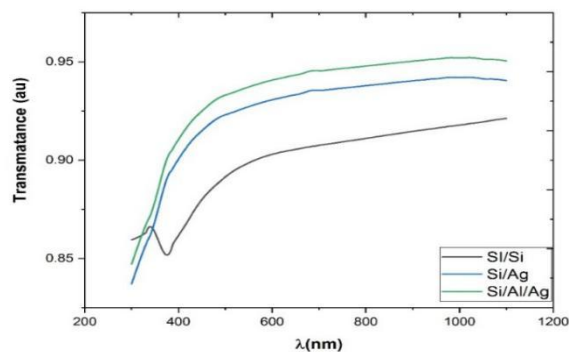

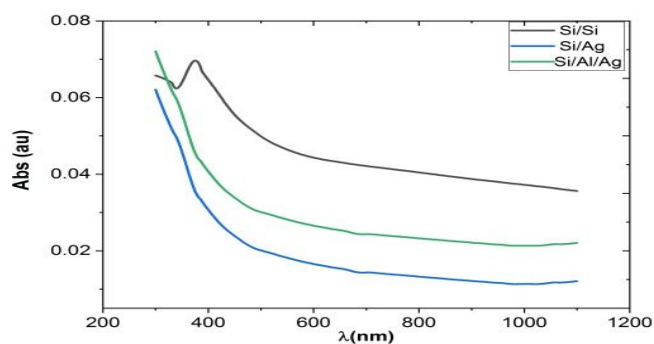Fig. 4 Optical transmittance spectrum of samples Si/Si, Si/Ag, and Si/Al/Ag.

Fig. 5 Absorbance spectra of Si/Si, Si/Ag, and Si/Al/Ag multilayers.

_____

To determine the direct optical band gap, $(\alpha h\upsilon)^2$ is plotted verse the photon energy ($h\upsilon$), as seen in Fig. (6.a). The direct optical band gap value is determined by extrapolating the linear fitted lines on the higher axis in these data points and tabulated in Table (2). It is observed that the optical band gap values are 1.50, 1.6, and 1.53 eV for (Si/Si), (Si/Ag), and (Si/Al/Ag), respectively. The variations in band gap values for doped a-Si occur because the introduction of dopants alters the electronic structure. The changes depend on the concentration of the dopant and whether it introduces new energy levels within the band gap. The band gap of the material could potentially be increased or decreased based on the influence of doping on its electronic structure and the duration of annealing.

The Urbach energy E_u was determined employing the subsequent [20]eq. (2).

$$\alpha = \alpha_0 \exp(h\upsilon/E_u) \qquad (2)$$

where α is the absorption coefficient and α_0 is a constant,h Planck constant and υ is the frequency. Fig. (6. b) illustrates the dependence of Ln (α) on (hυ). The values of E_u were calculated by fitting eq (2) and shown in Table (3). This indicates that the degree of structural disorder of nanocomposites has increased. Hence, it contributes to the localized states increasing and the optical band gap decreasing. The enhancement in prepared samples properties is reported in Table (2).

Table (2) Optical band gap values and Urbach energy for Si/Al/Ag multilayers.

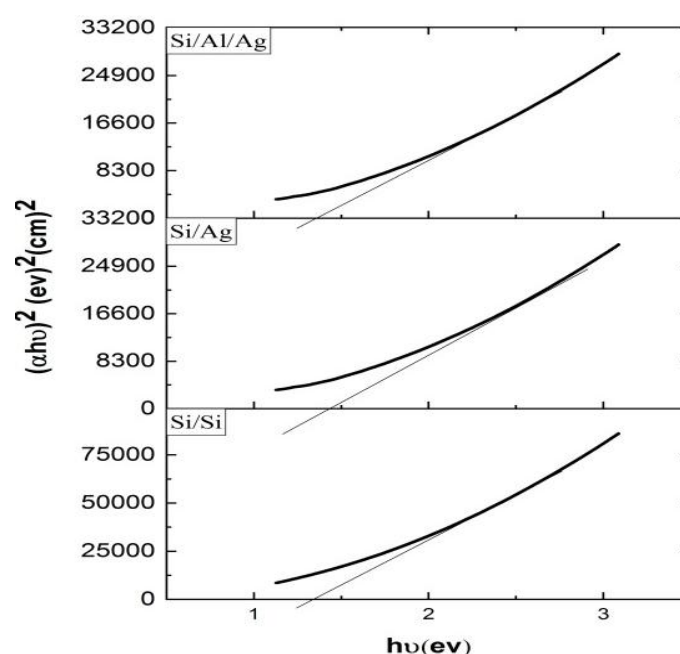| Sample	Direct Band Gap (ev)	Urbach energy (mev)
Si/Si	1.5	60
Si/Ag	1.6	60
Si/Al/Ag	1.53	70

Fig. 6 Dependence of (a) αhυ2 and (b) (lnα) vs (hυ) of multilayers Si/Si, Si/Ag, and Si/Al/Ag.
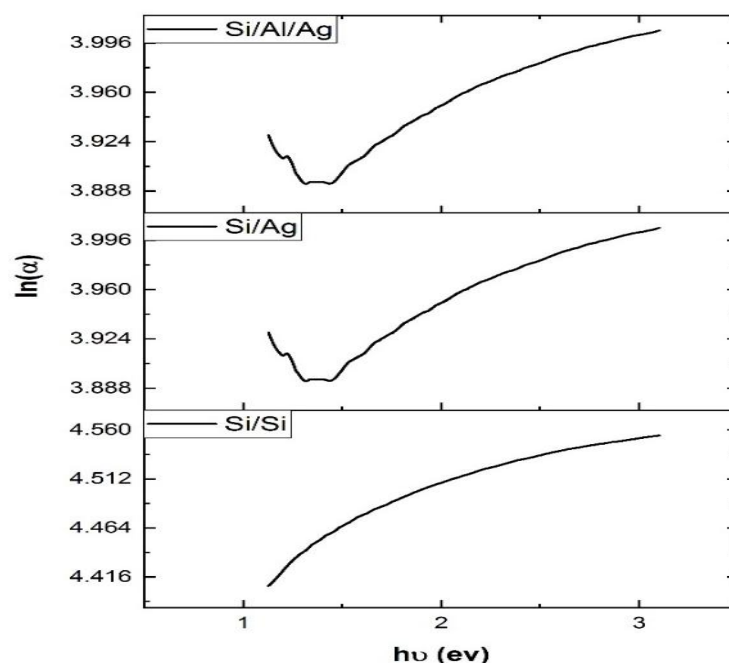
Fig. 7 shows an estimated extinction coefficient for the thin films of Si/Si, Si/Ag, and Si/Al/Ag. Calculation of the extinction coefficient was done using the measured absorption spectrum[21]:

$$K = \alpha\lambda/4\pi \qquad \qquad (3)$$

where α is the measured absorption.

Fig.7 shows the extinction coefficient (K) values as a function of wavelength for Si/Si, Si/Ag, and Si/Al/Ag multilayer films. It is clear that the values of K are decreasing by adding Ag and Al on the Si layers due to decreasing in the absorption coefficient (see Fig.6). Since the light travels through these different layers, reflections occur at each interface, which leads to decreasing the absorption coefficient. For Si/Si films, the large band gaps of silicon, aluminum, and silver oxide multilayers require higher energy to excite electrons across the band gap, resulting in lower K values. Additionally, the interfaces between layers can reduce scattering losses, potentially decreasing the overall extinction coefficient. In contrast, for the Si/Ag and Si/Al/Ag samples, the extinction coefficient decreases because these materials possess smaller band gaps, allowing electrons to be excited with minimal energy. Consequently, the refractive index of these samples increases, enhancing their optical properties due to the presence of silicon, aluminum, and silver with their lower energy requirements for electron excitation.

Fig. (8) shows the refractive index of the prepared samples as a function of wavelength for Si/Si, Si/Ag, and Si/Al/Ag multilayers. The low n value for Si/Ag and Si/Al/Ag multilayers is due to their free electron contribution to the optical response. Metals are highly reflective and their free electrons can screen the electric field of light, reducing the effective refractive index. The optical dispersion parameters such as E_o (the average energy gap), E_d (the dispersion energy), and n_o (the refractive index at infinite wavelength) are crucial for understanding the optical properties of multilayer materials. These parameters can be obtained using methods like spectroscopic ellipsometry or fitting the optical spectra to models such as the Wemple-DiDomenico single-effective oscillator model. The specific values for Si/Si, Si/Ag, and Si/Al/Ag oxide multilayers will depend on various factors, including layer thickness, interface quality, fabrication methods, and the presence of oxide layers [22].
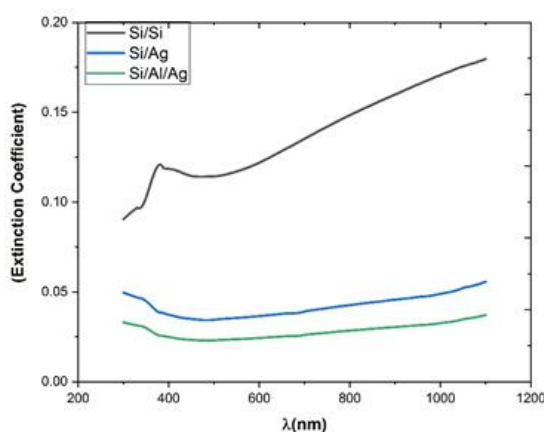
Fig. 8 The extinction coefficient spectrum of Si/Si, Si/Ag, and Si/Al/Ag multilayers.

The refractive index below the inter-band absorption edge according to the Wemple-Di Domenico single oscillator model [23] is given as follows:

$$n^2 = 1 + \frac{E_d E_0}{[E_0^2 - (h\upsilon)^2]} \quad (4)$$

where E_o and E_d are the single-oscillator energy and dispersion energy parameters respectively. By plotting $(n^2-1)^{-1}$ vs $(h\upsilon)^2$ and fitting the data, a straight line is obtained as shown in Fig. (9), E_o and E_d are determined directly from the gradient, $(n^2-1)^{-1}$ and the intercept (E_o/E_d), on the vertical axis [24]. The single-oscillator parameters for the thin films have been calculated and discussed in terms of the Wemple-Di Domenico model. From Equ.4 one can calculate the no the static refractive index.

$$n_0 = \sqrt{\left(1 + \frac{E_d}{E_0}\right)} \quad\quad (5)$$

Ed values changees with changing the metals, and the rise in E_0 values are due to the different metals in the multilayers which are given in Table (3) [25].

Table (3): The optical dispersion parameters of Si/Si, Si/Ag, and Si/Al/Ag multilayers

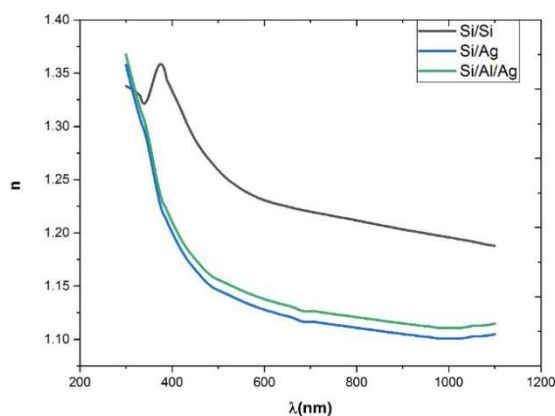| Sample	E_0 (ev)	E_d (ev)	n_0
Si/Si	1.79	4.65	1.89
Si/Ag	0.96	4.5	2.38
Si/Al/Ag	0.95	4.4	2.37

Fig. 9 Reflective index as a function of optical wavelength for Si/Si, Si/Ag, and Si/Al/Ag multilayers.
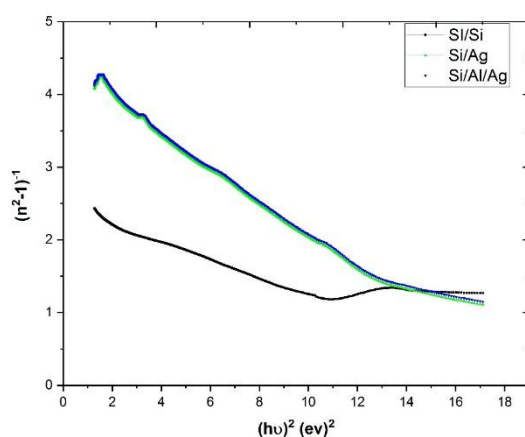
Fig. 10 The relation between $(n^2 - 1)^{-1}$ versus $(h\upsilon)2$ for Si/Si, Si/Ag and Si/Al/Ag.

Temperature dependence of AC conductivity:

The temperature dependence of the total AC conductivity ($\sigma_{total}(\omega)$) at various frequencies for the deposited multilayers of Si/Si, Si/Ag, and Si/Al/Ag is illustrated in Fig (10). It is clear that the total conductivity increases with increasing the temperature of the different samples. The shape of the curve suggests two different regimes with different activation energies the first with low temperature dependence and the other with high temperature dependence. The activation energy, E_a, for AC conduction was determined using the Arrhenius equation Equ. (6) and the least squares method[26]. The calculated activation energy values are listed in Table 4.

$$\sigma_{total} = A\exp\left(\frac{-E_a}{k_BT}\right) \qquad (6)$$

where A is the pre-exponential factor and E_a is the activation energy, and k_B is the Boltzmann constant. Additionally, the conductivity values of all samples show changes with temperature, indicating a phase transition within the measured temperature range. This reveals two distinct regions at relatively low and high-temperature ranges respectively. It is also noted that the activation energy in the first region, ΔE_a lies in the range of 0.7-1.9 eV, and the second region from 2.2 to 1.2 eV. The behavior of the activation energy values across these two conduction regions does not exhibit regular changes with the variation in elements as a result of the oxidation process and eutectic phase transition [27].
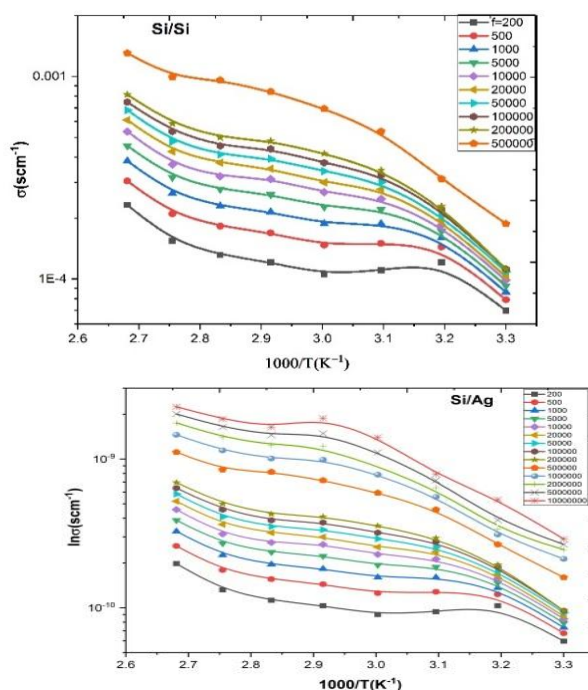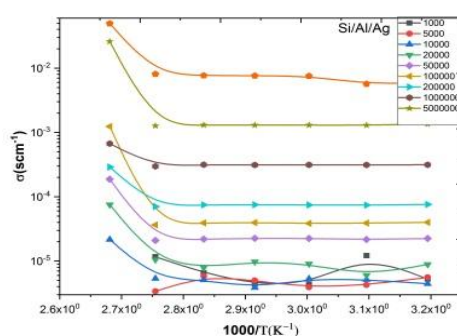
Fig. 11 Variation of ln (σ_{AC}) with 1000/T at different frequencies Si/Si, Si/Ag, and Si/Al/Ag samples multilayers

Table (4): Obtained values of the activation energy of the AC conductivity for Si/Si, Si/Al, Si/Ag, and Si/Al/Ag multilayer films at different frequencies.

Sample	10KHz	50KHz	500 KHz	10 KHz	50 KHz	500 KHz
	ΔE_{ac1}, eV			ΔE_{ac2}, eV		
Si/Si	0.96	0.95	0.741	2.27	2.4	2.22
Si/Ag	0.65	0.69	0.5	2.3	2.13	2.1
Si/Al/Ag	2.19	2.1	1.91	1.9	1.7	1.2

Frequency dependence of total Conductivity of Si/Al/Ag multilayers:

The AC conductivity $\sigma_{AC}(\omega)$ for all the amorphous semiconductors increases with frequency, Fig. (11) illustrates the frequency dependence on total electrical conductivity for Si/Si, Si/Ag, and Si/Al/Ag multilayers over a temperature range of 303 to 373 K and a frequency range of 100 Hz to 500 kHz. At low frequencies, the conductivity represents σ_{DC}, and as the frequency increases, it shows the frequency dependence of σ_{AC} for all samples. There is a clear, sharp linear increase with frequency, attributed to the increased mobility of charge carriers. This behavior adheres to the universal power law [28,29],

$$\sigma_{total}(\omega) = \sigma_{DC} + \sigma_{AC} \qquad (7)$$
$$\sigma_{AC} = A\omega^s$$

where σ_{DC} is the direct current conductivity, A is frequency independent pre-exponential factor, ω is the angular frequency and s is the angular frequency power. The conductivity increases with increasing frequency, the same behavior of the frequency dependence of $\sigma_{AC}(\omega)$ was obtained for all the investigated samples. The general behavior of σ_{total} versus frequency can be explained by Equ. (7), where the second term ($A\omega^s$) dominates at the higher frequency range. The values of s have been determined by the least square fitting and listed in Table (5). Fig. (12) shows the temperature dependence of s power, the behavior for Si/Al/Ag is a sharp decrease followed by a sharp increase which agrees with the tunneling effect behavior. As temperature increases, the vibrations of atoms within the material also increase, leading to a higher probability of electron tunneling between energy levels [30]. On the other hand, Si/Ag and Si/Al/Ag decrease with increasing temperature, the S power of the conduction mechanism can be understood based on the correlated barrier hopping model (CBH) where (0.5 < S < 1), when S greater than 1 refer to tunneling model, the exponent S decreases with increasing T according to the Equ. (8) [31,32].

$$s = 1 - \left[\frac{6K_B T}{W_M}\right] \qquad (8)$$

where W_M is the maximum barrier height.

In disordered systems, the AC conductivity often arises from the hopping of charge carriers between localized states. The frequency dependence can be understood in terms of the time scale for hopping. At higher frequencies, the charge carriers can respond more quickly, leading to increased conductivity [33].

The S value of (0.2) for (Si/Si, Si/Ag) suggests that the material has a relatively low level of disorder and that the charge carriers face lower energy barriers for hopping or tunneling. Such low S values are often observed at lower frequencies where long-range hopping or tunneling processes dominate. The temperature dependence of

the AC conductivity can also influence the S value. At higher temperatures, thermal activation may reduce the dominance of low-energy hopping or tunneling, potentially altering the S value [34, 35].

When the S value is about 1.5, it typically indicates a more complex conduction mechanism involving long-range interactions or correlated hopping processes. This value is higher than 1, which suggests a significant contribution from interactions between carriers or with the lattice structure [36, 37]. Fowler-Nordheim (F-N) tunneling is a quantum mechanical tunneling process that occurs at high electric fields, allowing electrons to tunnel through a triangular potential barrier. It is particularly relevant in thin films, metal-oxide-semiconductor structures, and field-emission devices. Here's a detailed explanation of the F-N tunneling mechanism which occurs under the influence of a high electric field, this field distorts the potential barrier making it thinner and more triangular, which facilitates tunneling. The potential barrier that electrons must tunnel through becomes triangular due to the applied electric field. The barrier height is determined by the work function of the material, which is the energy required for an electron to move from the inside of the material to just outside it [38].

Table (5): Extracted values of S for Si/Al/Ag samples multilayers

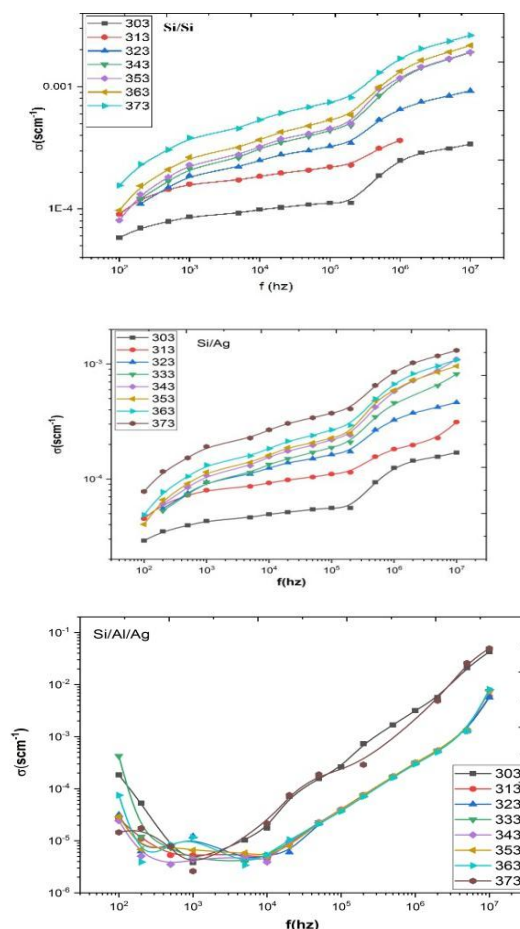| Temperature	Sample/s power	Sample	Sample
T(K)	Si/Si	Ag/Si	Ag/Si/Al
323	1.16	0.16	2.46
333	1.05	0.22	2.39
343	1.03	0.16	2.39
363	0.98	0.26	2.38
373	0.96	0.29	1.96

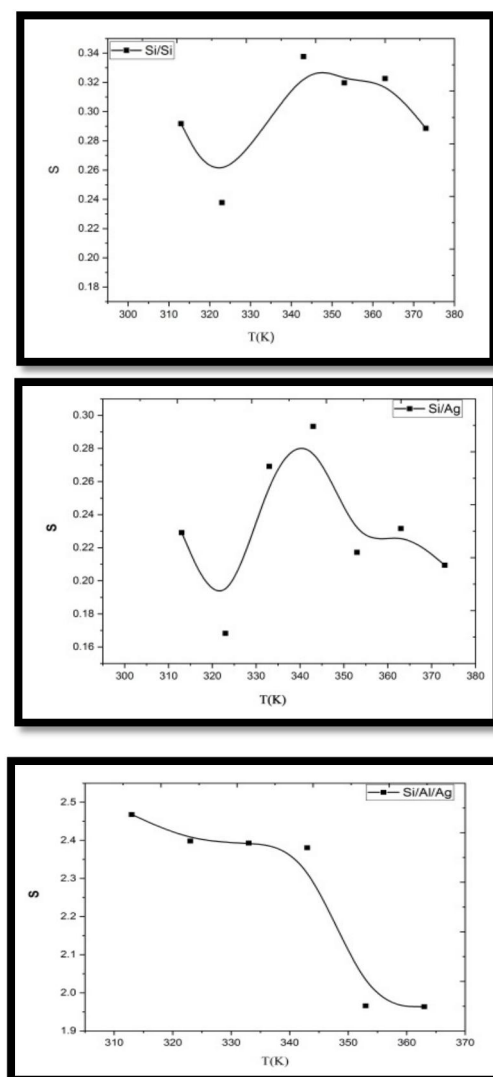Fig. 12 Frequency dependence of the total conductivity σ (ω) for Si/Si, Si/Ag, and Si/Al/Ag samples multilayers.

Fig. 13 Temperature dependence of the power *S* for Si/Si, Si/Ag, and Si/Al/Ag samples multilayers

Current-Voltage Characteristics of Si/Si, Si/Al, Si/Ag, and Si/Al/Ag Multilayers

Fig. (13) illustrates the current-voltage (I-V) characteristics at room temperature for both dark conditions and under white light illumination. The I-V curves demonstrate linearity up to an applied voltage of 20 V, indicating a direct proportionality between current (I) and voltage (V), consistent with Ohm's Law (I $\propto$ V). At low voltages, the linear region of the I-V curves suggests that the current is primarily governed by carriers generated during photo-irradiation. This ohmic behavior can be attributed to the assumption that at low voltages, significant carrier injection from the electrode contact does not occur, and the initial current is dominated by the intrinsic motion of free carriers. Under standard temperature and pressure conditions, the primary charge carriers in a semiconductor are generated through light excitation. Silver oxide semiconductor nanoparticles, having a small energy band gap, require minimal energy to excite electrons from the filled valence band to the empty conduction band. [39, 40]. The resistance in the dark RD and exposure to light RL are 37 and 30 Ω respectively. The Photosensitivity was found to be 1.23.
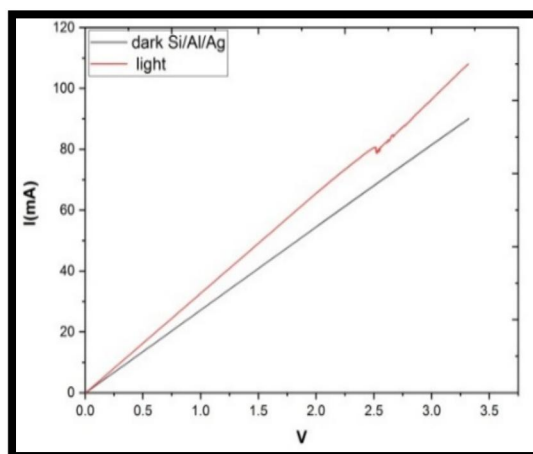
Fig. 14 (I.V) characteristic curve for Si/Al/Ag multilayers.

4. Conclusion

The study of amorphous silicon-metal multilayers, composed of silicon, aluminum, and silver, reveals their potential in optoelectronic applications due to their unique optical and electronic properties. The research emphasizes the importance of understanding oxidation mechanisms and their impact on the performance and stability of these multilayer structures. The study reveals that incorporating metals like aluminium and silver into the silicon matrix can manipulate surface plasmon resonance, leading to Strategies to mitigate oxidation-induced degradation, such as optimizing the fabrication process and employing protective coatings, are crucial for enhancing the long-term reliability and performance of amorphous silicon-metal multilayer-based optoelectronic devices.

5. Conflicts of interest

"There are no conflicts to declare".

6. References

1.	Polman A., Kociak M. and Javier García de Abajo F. Electron-beam spectroscopy for nanophotonics, Nature Materials, vol. 16, no. 10, pp. 1106-1107, 2017. Doi.org/10.1038/s41563-019-0409-1

2.	Green M. A., Ho-Baillie A., and Snaith H. J., The emergence of perovskite solar cells, Nature Photonics, vol. 8, no. 7, pp. 506-514, 2014. Doi: 10.1038/NPHOTON.2014.134

3.	Gao S., Zhou R, Samanta S., Junle Qu. , Tymish Ohulchanskyy Y. Recent advances in plasmon-enhanced luminescence for biosensing and bioimaging, Analytical Chemistry, vol. 1254, 8 May 2023, 341086. Doi.org/10.1016/j.aca.2023.341086

4.	Hirano p.T. , Kawamura M. , Kiba T., Yoshio Abe, Ho Kim K., Takeshi Hamano, Oxidation-induced changes in the optical properties of silicon-aluminum-silver multilayers, Surface and Coatings technology, vol. 28, no. 6, 2020. Doi.org/10.1016/j.surfcoat.2020.125752

5.	Wang R., Zhang Y., Li, et al .Q., Enhancing the stability of silicon-aluminum-silver multilayers against oxidation through surface passivation, Journal of Materials Chemistry C, vol. 26, no. 14, 2019.

6.	Macleod H. A., Sputtering methods for deposition of thin films, Handbook of Thin Film Deposition Processes and Techniques, 2nd Edition, William Andrew Publishing, 2002.Vol: 978-0-12-812311-9. Doi.org/10.1016/B978-0-12-812311-9.00001-3

7.	Nawwar M. A., Abo Ghazala MS, Sharaf El-Deen LM, Anis B, El-Shaer A, Elseman AM, Rashad MM, Kashyout AEB.RSC Adv. 2023 May 11;13(21):14472. Doi: 10.1039/d3ra90040a. eCollection 2023 May 9.

8.	Abo Ghazala, M. S., Othman, H. A., Sharaf El-Deen L. M., Nawwar M. A., Kashyout A. B. Fabrication of Nanocrystalline Silicon Thin Films Utilized for Optoelectronic Devices Prepared by Thermal Vacuum Evaporation. ACS omega vol. 5,42 27633-27644. 16 Oct. 2020

9.	Nawwar M.A., Abo Ghazala M. S., Sharaf El-Deen L. M., Kashyout A. B. Impact of strain engineering and Sn content on GeSn heterostructured nanomaterials for nanoelectronics and photonic devices. RSC Adv. 2022 Aug 30; 12 (38) : 24518-24554. Doi: 10.1039/d2ra04181b.

10.	Dionne J. A., Sweatlock L. A., Atwater H. A., and Polman A., Plasmon slot waveguides: Towards chip scale propagation with subwavelength scale localization, Physical Review B, vol. 73, no. 3, 2006. Doi.org/10.1103/PhysRevB.73.035407

_____

11.   Oulton R. F., Sorger V. J., Genov D. A., Pile D. F. P., and X. Zhang, A hybrid plasmonic waveguide for subwavelength confinement and long-range propagation, Nature Photonics, vol. 2, no. 8, pp. 496-500, 2008. Doi/10.1038/nphoton.2008.131

12.   Levine Z. H., and Ravel B. Identification of materials in Integrated circuit interconnects using X-ray absorption near-edge spectroscopy. Journal of Applied Physics. (1999); 85(558):81-98. Doi.org/10.1063/1.369489

13.   Mott N. F., Davis E. A. Electronic Processes in Non-Crystalline Materials. Oxford University Press (1979).ISBN97-0-19-964533-6 (Pbk).13579108642

14.   Austin I. G., Mott N. F., Polarons in Crystalline and Non-Crystalline Materials. Advances in Physics, (1969). 18(71), 41-102. Doi.org/10.1080/00018736900101267

15.   Ibach H., Lüth H., Dielectric Properties of Materials An Introduction to Principles of Materials Science Solid-State Physics: Springer ISBN 978-3-540-93803-3 (2009). Doi: 10.1007/978-3-540-93804-0

16.   Feiffer H. P., Wang C. Nanoscale Res. Rodolfo Cisneros, Lett (2010) 5:686–691. Doi 10.1007/s11671-010-9532-2

17.   El-Desouky H., Hassan S., El -Shaer A., Abo Ghazala M. S., Elrasasi T. Y. Preparation and characterization of amorphous multi layers of Silicon Al and Ag Egypt J. Solids, Vol. (46) (2024)

18.   Chen C., Huang X., Qin W. Preparation, characterization and thermal decomposition of polyimides with main chain containing cycloaliphatic units. J Macromol Sci B. Vol. 47, 2007-Issue1 Doi.org/10.1080/00222340701746093

19.   Ricardo A.Marques Lameirinhas; João Paulo N. Torres, António Baptista,Maria João Marques Martins, (2022). "A new method to analyse the role of surface plasmon polaritons on dielectric-metal interfaces". IEEE Photonics Journal. 14 (4): 1-9. Bibcode:2022IPhoJ..1481967L. Doi:10.1109/JPHOT.2022.3181967 .

20.   J.Tauc, (1970-08-01). "Absorption edge and internal electric fields in amorphous semiconductors". Materials Research Bulletin. 5 (8): 721–729. Doi:10.1016/0025-5408(70)90112-1. ISSN 0025-5408.

21.   Forouhi.A.R;Bloomer.I, (1986). "Optical Dispersion Relations for Amorphous Semiconductors and Amorphous Dielectrics". Physical Review B. 34 (10): 7018–7026. Bibcode:1986PhRvB..34.7018F. Doi:10.1103/physrevb.34.7018. PMID 9939354.

22.   Dmitruk N. L., Korovin A.V., Physical Nature of Anomalous Optical Transmission of Thin Absorptive Corrugated Films Vol. 89, No. 2, pp. 68–72. Pleiades Publishing, Ltd., 2009. Doi: 10.1134/S0021364009020040

23.   Al-Kuhaili M. F. Characterization of thin films produced by the thermal evaporation of silver oxide 2007 J. Phys. D: Appl. Phys. 40 2847
Doi. 10.1088/0022-3727/40/9/027.

24.   Dmitruk N. L., Korovin A.V., Physical Nature of Anomalous Optical Transmission of Thin Absorptive Corrugated Films Vol. 89, No. 2, pp. 68–72. Pleiades Publishing, Ltd., 2009. Doi: 10.1134/S0021364009020040

25.   Mahendiaa S. Tomar A. K., Kumar S., Alloys J. Compd. 2010, 508,406–411.
Doi:10.1016/j.jallcom.2010.08.075.

26.   Yuguo T. , Sergey V. , Oliver K., Zi Ouyang , Johnson W., Thomas S., Michael W., Renate E."Effect of annealing temperature on crystallization Kinetic, film properties and cell performance of silicon thin-film solar cells on glass."Solar Energy Materials and Solar Films 451:334-339(2004). Doi.org/10.1016/j.solmat.2012.01.039

27.   Westbrook J. H., Fleischer R. L. Collection of Phase Diagrams. Intermetallic Compounds Principles and Practice, Volume 3: Progress. Edited by J. H. Westbrook, R. L. Fleischer Copyright & 2002 John Wiley & Sons Ltd
ISBNs 0-471-49315-5 (Hardback); 0-470-84585-6 (Electronic)

28.   Garrett P. D, Grubb D. T. Effect of drawing on the α relaxation of poly (vinyl alcohol) J. Poly. Sci. B. 1988;26:2509. Doi.org/10.1002/polb.1988.090261209

29.   Ioannis K., Brian S., and Stephen J. Guy
Phys. Rev. Lett. 113, 238701 – Published 2 December,2014.DOI.org/10.1103/PhysRevLett.113.238701.

30.   Bardeen J. , Cooper L. N. , and Schrieffer J. R. Theory of Superconductivity, Phy. review. jornal, American Physical Society,1957 Vol E 108, number 5, Doi:https://doi.org/10.1103/PhysRev.108.1175

31.   Lee C., Lee S., Sul C. and Bae S., Frequency dependence of AC conductivities of KNb1−xVxO3 single crystals Physica B 239 (1997) 316. Doi.org/10.1016/S0921-4526(97)00340-2

32.   Long A. R., Frequency-dependent loss in amorphous semiconductors Adv. phys 31 (1982) 553. Doi.org/10.1080/00018738200101418

33.   Mott N. F. and Davis E. A., Hopping conductivity in amorphous and disordered materials, Electronic Processes in Non-Crystalline Materials, 2nd Edition, Oxford University Press (1979) ISBN: 978-0198505500.

_____

34.   Ghosh A. AC conductivity and dielectric relaxation in amorphous semiconductors and disordered systems Advances in Physics, 31, 553 (1982)
Doi: 10.1080/00018738200101479

35.   Homes C. C., Timusk T., and Clayman B. P., AC conduction in disordered solids: beyond the universal dielectric response , Physical Review B, 43, 9869 (1991)
   Doi: 10.1103/PhysRevB.43.9869

36.   Anderson P. W. and Hasegawa H., AC conductivity in chalcogenide glasses: a quantum mechanical tunneling approach Physical Review, 100, 675 (1955)
Doi: 10.1103/PhysRev.100.675

37.   Macdonald J. Generalizations of universal dielectric response and a general distribution of activation energies model for dielectric and conducting systems, J. of App. Phy. 1985 Physic. Doi:10.1063/1.336004

38.   Ben Taher Y., Oueslati A., Maaloul N. K., Khirouni K., Gargouri M., Conductivity study and correlated barrier hopping (CBH) conduction mechanism in diphosphate compound Applied Physics A, vol. A (2015) 120:1537–1543
Doi: 10.1007/s00339-015-9353-3

39.   Tawfik E. K., Fawzy Y. H. A., El-Ghazaly M. H. and Ashry H. A. Study of the DC-electrical properties of a novel polyvinyl alcohol/Ag hybrid nanocomposites netjournals. Vol. 3(2), pp. 26-36, June 2015 ISSN: 2437-1300

40.   El-amir A. A. M., Ohsawa T., Nabatame T., Ohi A., Wada Y., Nakamura M., Shimamura X. Fu, K., and Ohashi N., Mater.Silicon-compatible Mg2Si/Si n-p photodiodes with high room temperature infrared responsivity Sci. Semicond. 2019.
Doi.org/10.1016/j.mssp.2019.06.012